What the hippocampus tells the HPA axis: Hippocampal output attenuates acute stress responses via disynaptic inhibition of CRF+ PVN neurons

Anthony B. Cole [a,b,c], Kristen Montgomery [a,d], Tracy L. Bale [d,e], Scott M. Thompson [c,e,f,*]

[a] Program in Neuroscience, University of Maryland School of Medicine, Baltimore, MD, 21201, USA
[b] Medical Scientist Training Program, Departments of University of Maryland School of Medicine, Baltimore, MD, 21201, USA
[c] Physiology, University of Maryland School of Medicine, Baltimore, MD, 21201, USA
[d] Pharmacology, University of Maryland School of Medicine, Baltimore, MD, 21201, USA
[e] Psychiatry, University of Maryland School of Medicine, Baltimore, MD, 21201, USA
[f] Department of Physiology, University of Maryland School of Medicine, 655 W. Baltimore St., Baltimore, MD, USA

ARTICLE INFO

ABSTRACT

The hippocampus exerts inhibitory feedback on the release of glucocorticoids. Because the major hippocampal efferent projections are excitatory, it has been hypothesized that this inhibition is mediated by populations of inhibitory neurons in the hypothalamus or elsewhere. These regions would be excited by hippocampal efferents and project to corticotropin-releasing factor (CRF) cells in the paraventricular nucleus of the hypothalamus (PVN). A direct demonstration of the synaptic responses elicited by hippocampal outputs in PVN cells or upstream GABAergic interneurons has not been provided previously. Here, we used viral vectors to express channelrhodopsin (ChR) and enhanced yellow fluorescent protein (EYFP) in pyramidal cells in the ventral hippocampus (vHip) in mice expressing tdTomato in GABA- or CRF-expressing neurons. We observed dense innervation of the bed nucleus of the stria terminalis (BNST) by labeled vHip axons and sparse labeling within the PVN. Using whole-cell voltage-clamp recording in parasagittal brain slices containing the BNST and PVN, photostimulation of vHip terminals elicited rapid excitatory postsynaptic currents (EPSCs) and longer-latency inhibitory postsynaptic currents (IPSCs) in both CRF+ and GAD + cells. The ratio of synaptic excitation and inhibition was maintained in CRF + cells during 20 Hz stimulus trains. Photostimulation of hippocampal afferents to the BNST and PVN in vivo inhibited the rise in blood glucocorticoid levels produced by acute restraint stress. We thus provide functional evidence suggesting that hippocampal output to the BNST contributes to a net inhibition of the hypothalamic-pituitary axis, providing further mechanistic insights into this process using methods with enhanced spatial and temporal resolution.

1. Introduction

The corticosteroid neuroendocrine response is controlled by the hypothalamic-pituitary-adrenal (HPA) axis (for review (Spencer and Deak, 2017; Russell and Lightman, 2019; Bale and Vale, 2004; Vale et al., 1981)). Corticotropin-releasing factor (CRF)-releasing neurons in the paraventricular nucleus of the hypothalamus (PVN) are the final common site upon which central projections from stress-sensitive brain regions converge to modulate HPA axis activity. CRF reaches corticotropes in the pituitary gland through the hypophyseal-portal circulation and stimulates the release of adrenocorticotropic hormone (ACTH), which then enters systemic circulation. Cells within the adrenal cortex are stimulated by ACTH binding to the Melanocortin receptor type 2 to synthesize and release glucocorticoids into circulation. The end product of HPA activation is the rapid production of glucocorticoids that have powerful and systemic effects on numerous systems throughout the body. The production of glucocorticoids therefore also requires tight regulation, typically thought to occur through negative feedback via glucocorticoid receptor (GR) and mineralocorticoid receptor (MR)-expressing cells. The canonical actions of these intracellular receptors act via relatively slow genomic mechanisms. During an acute stress event in a healthy functioning HPA axis, peak glucocorticoid levels rise rapidly, peaking within 30 min of stress onset, and return back to baseline within 120 min via negative feedback (Spencer and Deak, 2017). Numerous clinical manifestations can develop when glucocorticoids are chronically elevated or inadequately controlled, including central fat deposits,

hair loss, loss of bone density, and psychiatric manifestations (Sharma and Nieman, 2011; Ronchetti et al., 2018). Hyper-activation of the HPA axis is seen in a subset of patients with major depressive disorder, hypo-activation of the HPA axis is found in some PTSD patients, and HPA axis dysregulation has been suggested to be an etiological factor in the genesis of both (Pariante and Lightman, 2008; Holsboer, 2000; Kvarta et al., 2015; Kathol et al., 1989; Sonino and Fava, 2001).

GR and MRs are differentially expressed throughout the brain but are concentrated in regions thought to be responsible for mediating responses to stressful conditions. The ventral hippocampus (vHip) and subiculum carry affective information, display high levels of MR/GR, and have been implicated in HPA regulation (Bertagna et al., 2020; Fanselow and Dong, 2010; O'Mara, 2005; Lowry, 2002; Mueller et al., 2004; Herman et al., 1992; Maggio and Segal, 2009). In support of this hypothesis, lesioning the vHip or major hippocampal efferent tracts leads to alterations in the responses to acute stressors (Herman et al., 1998; Herman and Mueller, 2006) and an inability of exogenous corticosteroids to suppress HPA activation (Magarinos et al., 1987). Genetic deletion of GRs in cortical and hippocampal pyramidal cells also results in an elevation of circulating glucocorticoids (Herman et al., 1998).

The output of hippocampal pyramidal cells is glutamatergic and should excite CRF cells in the PVN if they are synaptically connected. It is suggested that an interposed population of GABAergic cells reverses this excitatory drive to inhibit the HPA axis. Electrophysiological studies have identified several candidate brain regions with a high density of inhibitory neurons that project to the PVN (Boudaba et al., 1996), but to our knowledge there is no physiological evidence demonstrating that these cells are both excited by hippocampal output and inhibit PVN cells. The bed nucleus of the stria terminalis (BNST) is one such candidate region (Cullinan et al., 1993, 2008; Herman and Cullinan, 1997; Avery et al., 2014; Gergues et al., 2020). It has dense expression of GAD+ and CRF + neurons and is positioned to integrate many stress-relevant signals and relay them to the PVN (Herman and Cullinan, 1997; Avery et al., 2014; Radley and Sawchenko, 2011; Lebow and Chen, 2016). Lesions and optogenetic manipulations within different subnuclei or subregions of the BNST have varying effects on HPA response (Lingg et al., 2020; Johnson et al., 2016, 2019; Choi et al., 2007). Our study uses this groundwork to guide our investigation into how exactly the hippocampus regulates the HPA axis and which intermediate brain regions may play a role.

2. Methods

All procedures were approved by the University of Maryland School of Medicine Institutional Animal Use and Care Committee and performed in accordance with the National Institutes of Health Guide for the Care and Use of Laboratory Animals.

2.1. Animals and housing

Male and female mice were group-housed with *ad libitum* access to water and standard rodent chow. Reporter mice were used for identification of the cell populations of interest by crossing Ai14 mice (B6; 129S6-*Gt(ROSA)26Sor^{tm14(CAG-tdTomato)Hze}*/J; Jackson Laboratory), for cre-dependent expression of tdTomato, with mice expressing cre recombinase under the control of the CRF (B6(Cg)-*Crh^{tm1(cre)Zjh}*/J; Jackson Laboratory) or glutamic acid decarboxylase (*Gad2^{tm2(cre)Zjh}*/J; Jackson Laboratory) promoters (Wamsteeker Cusulin et al., 2013; Morrison et al., 2020; Taniguchi et al., 2011; Madisen et al., 2010). Male and female mice were used for imaging and brain slice electrophysiological experiments, whereas only males were used for the experiments testing hippocampal activation on acute stress responses.

2.2. Viral injection

Stereotaxic surgery (Kopf stereotaxic apparatus) was performed at

5–6 weeks of age under 1.5–3% isoflurane anesthesia. AAV2 viral vectors were used to express channelrhodopsin and enhanced yellow fluorescent protein (EYFP)(AAV2-CAMKIIa-hChR2(H134R)-EYFP, UNC Viral Core) in Ca^{2+}/calmodulin-dependent kinase expressing neurons, likely pyramidal cells (Boyden et al., 2005; Wang et al., 2013). Viral solutions (0.5 μl, titer $1–8 \times 10^{12}$vg/ml) were injected bilaterally into ventral CA1 of the hippocampus (mm to Bregma: 3.3 AP, ±2.8 Lat, −3.8 D/V) at a rate of 0.1 μl/min. The syringe (Hamilton Neurosyringe, 33 gauge) was left in place for 10 min following final injection to allow for dispersal before withdrawing the syringe.

2.3. Imaging

Mice were sacrificed and brain tissue was collected 5–6 weeks following injection, allowing for expression and transport of ChR to distal axon terminals. Animals were transcardially perfused using 30 ml of phosphate-buffered saline (PBS, containing in mM: 137 NaCl, 2.7 KCl, 10 Na_2HPO_4, 1.8 KH_2PO_4), followed by 4% paraformaldehyde (PFA) in PBS. The brain was then extracted and mounted on to an agar base for vibratome sectioning. Brain slices for imaging were sectioned in either the coronal or parasagittal plane at a thickness of 75 μm on a Leica VT 1200S vibratome. Slices were washed in deionized water prior to slide mounting using Vectashield + DAPI. (Vector Laboratories, Burlington, CA) Images were taken on an Nikon Eclipse E600FN upright microscope (Fig. S1), Nikon W1 spinning disk confocal microscope fitted with Hamamatsu sCMOS camera (Fig. 1c,d,e), or Nikon Ti2-E inverted epifluorescence microscope fitted with a Spectra-X 7 channel LED light engine (Lumencor, Beaverton, OR) (Fig. 1a and b), as noted. Brain regions were referenced from the Mouse Brain Atlas and outlines from the atlas were used in the creation of anatomical images. (Allen Sagittal Images 19/21, Coronal Images 57/132, 59/132) (Daigle et al., 2018; Lein et al., 2007; Harris et al., 2019; Oh et al., 2014; Paxinos and Franklin, 2007) BNST subnuclei were identified using landmarks diagrammed in Lebow and Chen (2016) (Lebow and Chen, 2016) and based on a series of anatomical studies by Dong et al. (Dong et al., 2000, 2001; Dong and Swanson, 2003, 2004a, 2004b, 2006a, 2006b, 2006c).

2.4. Electrophysiology of hippocampal projections in vitro

Five to seven weeks after viral delivery of ChR-EYFP, mice were euthanized using isoflurane overdose and then perfused with critical recovery solution (CRS; in mM N-methy D-glucamine 92, KCl 2.5, NaH_2PO_4 30, HEPES 20, glucose 25, $CaCl_2$ 0.5, $MgCl_2$ 10) prior to decapitation (Ting et al., 2014). The brain was removed and mounted in ice-cold CRS during slicing. Coronal and parasagittal sections (300 μm thickness) were obtained, rested for 12 min, and then transferred to HEPES-buffered holding solution (NaCl 92, KCl 2.5, NaH_2PO_4 1.25, $NaHCO_3$ 30, HEPES 20, glucose 25, $CaCl_2$ 2, $MgCl_2$ 2) for 1 h prior to recording. Unless otherwise stated, all data shown were from slices taken in the parasagittal plane. Patch clamp recording was performed using Clampex 10.7 software, Digidata 1440 digitizer, and an Axopatch 200B amplifier (Molecular Devices, San Jose, CA). Pipettes were pulled to 4–10 mOhms using a Sutter Instruments P-87 micropipette puller and filled with a cesium methylsulphate-based pipette solution (concentrations in mM, $CsCH_3SO_4$ 135, $MgCl_6$–H_2O 2, HEPES 10, Mg-ATP 4, Na_2-GTP 0.3, Na_2-phosphocreatine 10, K_4-BAPTA 10). Slices were recorded in whole-cell voltage-clamp configuration in artificial cerebrospinal fluid (ACSF; in mM, NaCl 124, KCl 3, NaH_2PO_4 1.25, $NaHCO_3$ 26, glucose 20, $MgCl_2$ 1.5, $CaCl_2$ 2.5) bubbled with carbogen (95% CO_2, 5% O_2).

Optically evoked synaptic currents were elicited with a Prismatix BlueLED light source (Southfield, MI) (460 nm, 1 ms pulse duration 5–10 mW) delivered by an optical fiber with a 1000 μm diameter core (Thor Labs, Newton, NJ). The fiber was positioned with a micromanipulator to areas of dense EYFP expression near the junction of the fornix and BNST, as visualized with epifluorescence on the recording
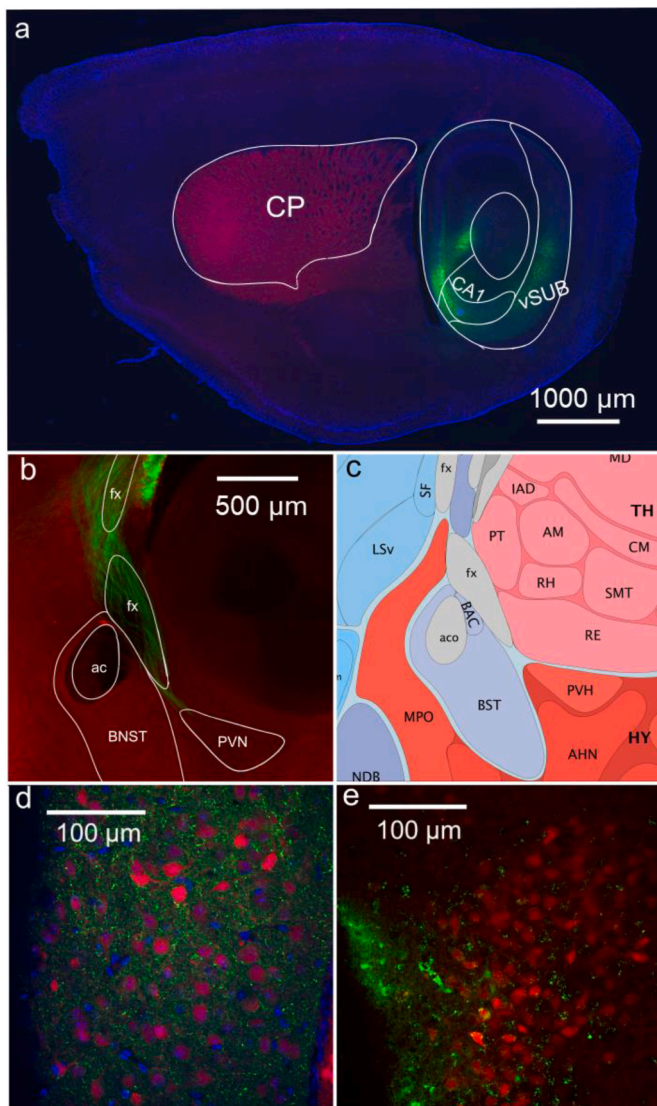
Fig. 1. Anatomy of ventral hippocampal terminals in GAD and CRF reporter mice.

a) EYFP (green) in glutamatergic pyramidal cells in the injection site in the ventral hippocampus and subiculum using an AAV2 virus with CAMKII-promoter driven expression in a GAD-tdTomato (red) mouse brain with DAPI counterstain (blue). Section sliced in the parasagittal plane and annotated with outlines from Allen Brain Atlas (sagittal view 2/21). **b)** Strong expression of EYFP (green) was seen in axons coursing through the fornix (fx), both anterior and posterior of the anterior commissure (ac), in a GAD-tdTomato (red) mouse. **c)** Diagram of nuclei in parasagittal sections of this region (Allen Mouse Brain Atlas and Allen Reference Atlas - Mouse Brain, sagittal view 19/21 image credit: Allen Institute for Brain Science https://atlas.brain-map.org/atlas?atlas=2#atlas=2&plate=100883858). **d)** Numerous hippocampal terminals (green) in the medial regions of the BNST in close proximity to GAD + neurons (red). **e)** Sparse hippocampal terminals expressing ChR2-EYFP (green) near CRF + neurons in the PVN in a coronal section from a CRF-tdTomato (red) mouse. (For interpretation of the references to colour in this figure legend, the reader is referred to the Web version of this article.)

setup. Electrically evoked currents were driven by direct stimulation of the fornix using a concentric bipolar electrode. Square current pulses of 1 ms duration and an intensity of 0.1–10 mA (World Precision Instruments Isostim A320, Sarasota, FL) were delivered either as single pulses at 0.1 Hz or as a train of pulses at 20 Hz, with 1 min between stimulus trains. The CsMeS-based internal pipette solution blocks K channels and facilitates clamping to depolarized holding potentials.

Conductances were calculated using the amplitude of the synaptic current divided by the driving force for the channels of interest (AMPAR-mediated current reversal potential = 0 mV, GABA$_A$R-mediated current reversal potential = −60 mV).

We recorded from 54 cells in slices from 25 CRF-tdTomato male and female animals. Optically evoked responses were obtained in only 8 cells in slices from 5 males and 3 females. We recorded from 26 cells in 19 GAD-tdTomato animals, with optically evoked responses obtained in only 7 cells in slices from 3 males and 4 females. The response amplitudes and probability of obtaining EPSCs and IPSCs were comparable in male and female slices and the data have therefore been pooled. There are a number of reasons why an optically evoked response may not have been elicited, including the underlying biology or the technical difficulty of the experiment, making interpretation of the lack of a response difficult.

2.5. Stimulation of hippocampal projections in vivo

Experiments were performed in male mice because the BNST is sexually dimorphic, and we were unable to find a description of the anatomy of the BNST in female mice to guide placement of the optical fiber. Optical fibers were constructed using a modified protocol as described by Sparta et al., 2012) (Sparta et al., 2012), using 0.22NA silica-core multimodal fiber (ThorLabs) epoxied into conical ceramic ferrules of 6.4 mm length and 127–131 μm bore (Precision Fiber Products, Chula Vista, CA). Fibers were polished using lapping sheets and tested using the LED system and an optical power meter to monitor output (OptoEngine PSU-III OptoEngine LLC, Midvale, UT and ThorLabs PM100D). Fibers with <80% power transmission or poorly defined, non-concentric light output were discarded. Optical fibers were implanted into C57Bl/6 mice vertically, with the tip of the fiber targeting hippocampal efferent projections upstream of the BNST, with coordinates (mm to Bregma: 0 AP, ±1.2 Lat, 3.8 D/V). This location likely did not result in stimulation of any fibers within the stria terminalis. Optical fibers were held in position using headcaps constructed of Den-mat dual-cure Geristore two-part dental cement (DenMat Holdings LLC, Ref 4506 and 03452410, Lompoc, CA). The skull was cleaned thoroughly and prepared with Vetbond (3M, Maplewood, Minnesota) to reduce skull moisture and promote skullcap adhesion. Fiber implants left a small but noticeable disruption of brain tissue that was apparent following fixation of brain, and this disruption was used for verification of fiber placement. After the completion of the experiment, animals were euthanized, and the brains were prepared for imaging as described in section 2.3. Following visual analysis, animals without both accurately targeted and high levels of hippocampal viral expression and appropriate fiber placement were excluded from the results (n = 2/9, 1/9 mice respectively). All imaging verification was done blinded to the experimental results.

Seven weeks were allowed following surgery for mice to recover and for the virus to fully express and transport ChR to distal axon terminals. Animals were singly housed two days prior to, and for the duration of, the experiment to minimize the stress of changing cage environment during the experiment as a source of variability. Animals were randomly assigned to either receive stimulation or mock stimulation on the first trial and then received the inverse treatment during their second trial, with at least one week separating trials in individual animals. All experiments were completed between 7:00 a.m. and 10:00 a.m. (0–3 Zeitgeber time) in order to reduce variability in circulating corticosterone (CORT) at baseline as well as minimizing baseline CORT levels (Spiga et al., 2014; Lightman and Conway-Campbell, 2010; Ikeda et al., 2013; Schouten et al., 2020).

On the day of the experiment, all setup of the optical stimulation and blood collection materials were prepared and made ready for use prior to any animal handling. Immediately prior to the stimulation session, the singly housed animal cages were quickly and carefully moved from their housing location to the experimental room. Animals were rapidly

withdrawn from their cage and immediately placed into the restraint device. The optical fibers were coupled to the light source and photostimulation and the timing of the restraint began. 1 ms pulses of light stimulation were given at 20Hz in 2 s intervals alternating between stimulation and no stimulation for 15 min 10 mW power at the implanted fiber tip was targeted based on measured power output of the light source on the day of the experiment and the fiber power percent transmission recorded prior to implantation (Ung and Arenkiel, 2012). The initial tail snip and blood was collected <3 min after initial handling of the animal's cage and used for baseline CORT measurements. Further blood collection was performed at 15, 30, 60, and 120 min after the initial collection.

2.6. HPA axis responsivity

Plasma corticosterone was measured following an acute 15 min restraint. Testing occurred 0–3 h after lights on. Tail blood from adult mice (n = 6 per condition) was collected at onset and completion of restraint (0 and 15 min, respectively) and 15, 45, and 75 min after the end of restraint (30, 60, and 90 min, respectively). Tail blood collection requires <30 s to complete. 5ul of blood was pipetted into 10ul of 50 mM EDTA buffer immediately following collection. Tubes were then centrifuged at 5000 rpm and plasma was stored at −80 °C until RIA analysis. Corticosterone levels were determined by ImmuChem Double Antibody Corticosterone ^{125}I-corticosterone Radioimmunoassay Kit for Rats and Mice according to kit instructions (MP Biomedicals, Santa Ana CA). A standard curve was generated for each run of RIA for 0–1000 ng/ml concentration, and ^{125}I counts were converted to CORT concentrations based on these curves. Samples were run in triplicate, with the average being used. Samples in which the raw counts from the gamma counter differed by > 1000 from replicate samples were discarded, and the average of the two remaining samples was used (7/270). Triplicates were each pulled from a single blood collection sample before RIA processing, so poor tail blood samples could lead to incorrect data. Therefore all cumulative CORT data from RIA was subjected to RObust regression and OUtlier removal (ROUT, Graphpad9) prior to analysis, and 2/60 samples were identified as outliers and excluded (Motulsky and Brown, 2006).

2.7. Statistics

Mixed-effects ANOVA and paired and unpaired t-tests were used to compare mean values between treatment groups where appropriate. For estimating CORT levels in control and treatment group over time, we performed a 2-way mixed method ANOVA, as the samples were taken as repeated measures but incomplete following outlier removal. Area under the curve calculations for the RIA data were performed using trapezoidal calculation based on the time between each sample and the calculated CORT value. Jitter was calculated using the standard deviation of the latency between optical stimulation and peak response. Because only one cell was recorded per slice, we treat each cell as an individual n. Statistics were computed in Prism 9 (Graphpad, San Diego, CA). All data were analyzed while blinded to experimental conditions.

3. Results

3.1. Distribution of hippocampal axon terminals

To identify potential brain regions that could function as an inhibitory relay for hippocampal regulation of responses, we first identified brain regions that 1) have high densities of GABAergic cells, 2) received excitatory inputs from the vHip, and 3) have known projections to PVN. Anatomical visualization of ventral hippocampal projections was performed by expressing ChR and EYFP in the ventral hippocampus in mice expressing the red fluorescent protein tdTomato in GAD-cre expressing interneurons (Fig. 1a, parasagittal section). Axonal projections from the

ventral hippocampus and subiculum were observed in the fornix, and dense terminal labeling was seen surrounding the anterior commissure within the bed nucleus of the stria terminalis (BNST) (Fig. 1b,c,d parasagittal sections). Similar projections were observed in the neuropil surrounding the PVN in the peri-PVN using the same ChR and EYFP injection scheme in a second line of mice expressing tdTomato in CRF-cre expressing neurons. There was little evidence of projections directly to the PVN itself (Fig. 1e, coronal section). Expression was primarily seen in the medial portions of the BNST, with some expression anterior to the anterior commissure, and more pronounced expression inferior and posterior to the anterior commissure. These anatomical findings led us to further interrogate the BNST and peri-PVN as potential relays between hippocampus and PVN.

3.2. Physiological responses to activation of hippocampal axonal terminals

Using the same injection scheme of ChR-EYFP into the ventral hippocampus, we measured optically evoked responses in CRF + neurons in the PVN. Coronal sectioning provided planes containing both EYFP-labeled terminals and tdTomato-expressing cells, indicating the presence of hippocampal terminals adjacent to cell bodies in the PVN in the peri-PVN. Cells were recorded using whole-cell voltage-clamp at holding potentials of 0 mV, the reversal potential for glutamatergic currents, and −60mV, the reversal potential for GABA$_A$ receptor mediated currents, to isolate optically evoked inhibitory postsynaptic currents (oIPSCs) and excitatory postsynaptic currents (oEPSCs), respectively. Optical stimulation was targeted at regions of dense EYFP expression near the fornix (Supplemental Figs. 1a and b). Stimulation of terminals in both peri-PVN and fornix in coronal sections failed to evoke any synaptic currents in CRF + cells at either potential (18 cells in slices from 6 animals). The failure to detect synaptic currents may have been because the axons were severed. We therefore repeated the experiments in brain sections prepared in the parasagittal plane, as shown in Boudaba et al., 1996) (Boudaba et al., 1996). In these parasagittal slices, oEPSCs and oIPSCs were recorded in CRF + neurons in response to photostimuli delivered to EYFP-positive terminals in the region of the fornix (Fig. 2a), suggesting that these axonal projection systems lie in a predominately anterior-to-posterior orientation that remains intact during parasagittal sectioning. As inhibition from the peri-PVN should remain intact in coronal sections whereas inhibitory projections from the BNST are more likely to be preserved in parasagittal sections, we suggest that hippocampal regulation of the PVN was more likely to be mediated by interposed neurons in the BNST and it was therefore the focus of our further experiments.

Within the PVN, stimulation of hippocampal fibers in the fornix elicited synaptic currents in CRF + neurons that were dominated by inhibition (Fig. 2a–d). The fraction of recordings in which an oIPSC was elicited (7 of 8 cells) was greater than the fraction in which an oEPSC was elicited (4 of 8 cells)(Fig. 2d). In experiments in which photostimulation elicited both oEPSCs and oIPSCs (3 of 8 cells), the mean amplitude and conductance of oIPSCs were not significantly different than for oEPSCs (Fig. 2c), although statistical comparisons are limited by the low number of cells with both. The IPSCs occurred with a significantly longer latency than EPSCs after photostimulation (Fig. 2b and c). The jitter in oIPSC measurements in CRF + cells was also 4-fold greater than for oEPSCs (Fig. 2c), although the low number of cells in which both EPSCs and IPSCs could be recorded (n = 3) prevented this difference from reaching statistical significance. We suggest that the excitation is monosynaptic whereas the inhibition is disynaptic.

We next recorded synaptic responses from GABAergic cells within the BNST. Photostimulation of hippocampal terminals elicited both oEPSCs and oIPSCs in GAD + cells (Fig. 2e–h). In contrast to the PVN, both oIPSCs and oEPSCs were elicited within the same cell in all 6 experiments (Fig. 2f,h). Furthermore, the mean amplitude and conductance of oEPSCs and oIPSCs were comparable in the BNST (Fig. 2g).
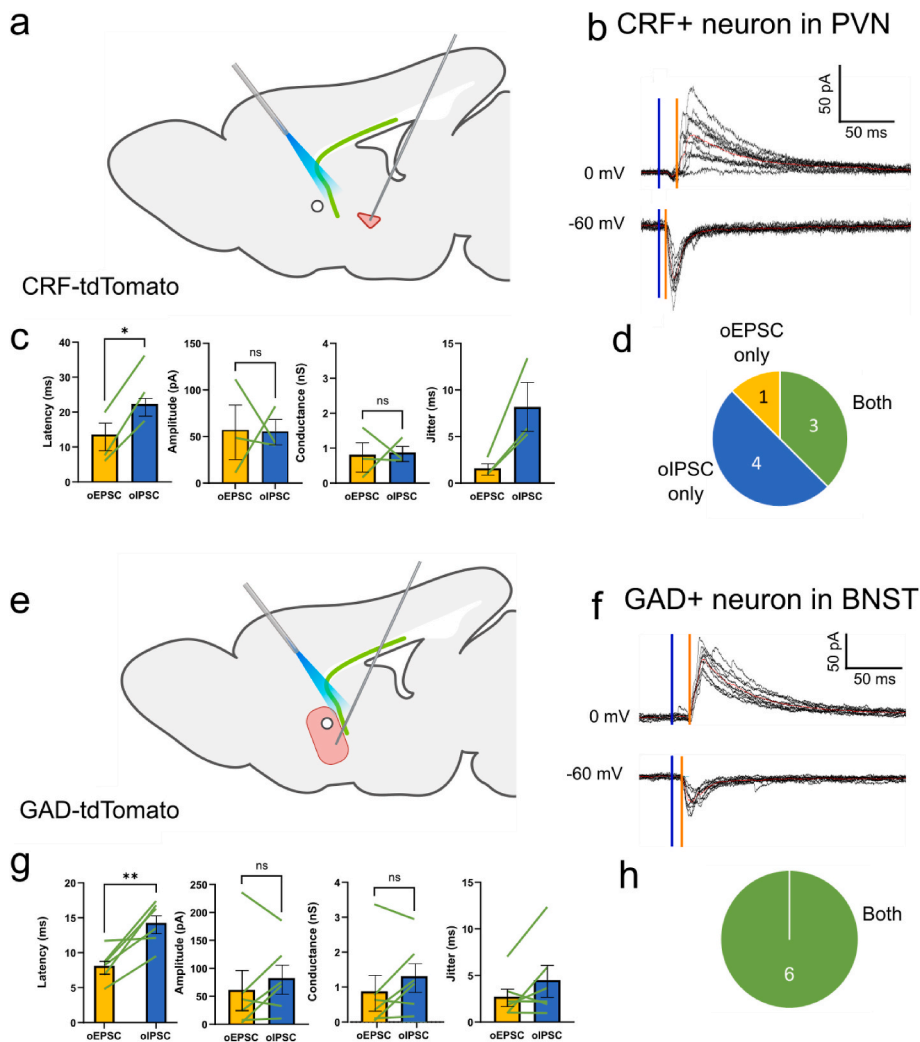
Fig. 2. Optically-evoked currents in CRF + neurons of PVN and GAD + neurons of the BNST. **a)** ChR and EYFP were expressed in CA1 pyramidal cells of the ventral hippocampus/subiculum in CRF-tdTomato reporter mice (male and female). **b)** Whole-cell voltage-clamp recordings from a CRF + neurons in the PVN. Photostimulation in the fornix elicited oEPSCs and oIPSCs at holding potentials of −60mV and 0 mV, respectively. Sample traces obtained with 10 stimuli delivered 1 min apart. Optical stimulation delivered at time indicated by blue bar and the latency to oIPSC (0 mV) and oEPSC (−60 mV) onset shown with orange bar. **c)** Pairwise comparison of oEPSCs and oIPSCs in single cells (n = 3) demonstrated an increased stimulus-response latency for oIPSCs compared to oEPSCs (p = 0.0162), but not significant differences in oEPSC and oIPSC amplitude or conductance. There was a large difference in jitter between oEPSCs and oIPSCs that did not reach statistical significance (p = 0.08). **d)** Number of cells in which oEPSCs, oIPSCs, or both were elicited. **e)** ChR and EYFP were expressed in CA1 pyramidal cells in GAD-tdTomato mice. **f)** Whole-cell voltage-clamp recordings from a GAD + inhibitory neuron in the BNST. Photostimulation in the fornix elicited oEPSCs and oIPSCs at holding potentials of −60mV and 0 mV, respectively. Optical stimulation delivered at time indicated by blue bar and the latency to oIPSC (0 mV) and oEPSC (−60 mV) onset shown with orange bar. **g)** There was an increased stimulus-response latency for oIPSCs compared to oEPSCs (n = 6, p = 0.0074), but no significant differences in oEPSC and oIPSC amplitude (n = 6, p = 0.3351) or conductance (n = 6, p = 0.1792). **h)** All six BNST cells recorded demonstrated both oEPSCs and oIPSCs. *, p < 0.05; **, p < 0.01. (For interpretation of the references to colour in this figure legend, the reader is referred to the Web version of this article.)

oIPSCs also had a longer latency than oEPSCs in the BNST, suggestive of monosynaptic excitatory stimulation and disynaptic inhibition, presumably by local inhibitory circuits within the BNST (Dong and Swanson, 2004a, 2004b, 2006a, 2006c; Kim et al., 2013).
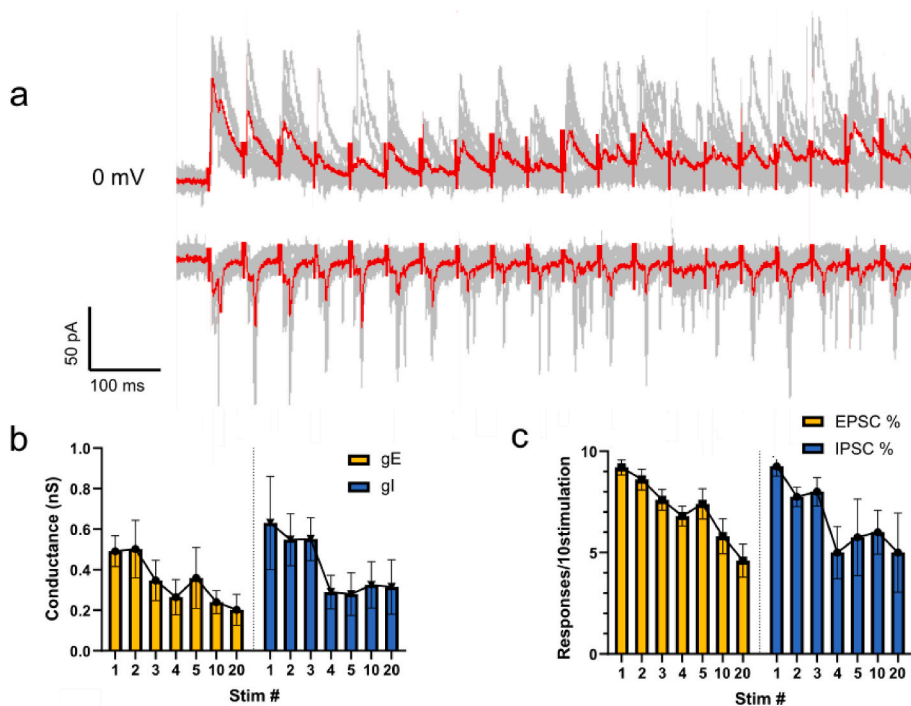
3.3. High frequency electrical stimulation

Activity in hippocampal inputs to the BNST and PVN *in vivo* is likely to occur at fairly high frequencies, and excitatory and inhibitory synaptic transmission display well-known activity-dependent dynamics (Larsen and Sjöström, 2015; Anwar et al., 2017). We therefore asked whether the ratio of excitation to inhibition was changed in a frequency-dependent manner in the PVN. Unlike optical stimulation, electrical stimulation of hippocampal afferents in the fornix produced both EPSCs and IPSCs in the majority of CRF + PVN cells recorded from (11 of 12) and was thus better suited to compare activity-dependent dynamics. We placed an electrode in the fornix of parasagittal brain slices and recorded electrically evoked responses in CRF + cells in the PVN using 20 Hz stimulation for 1 s bouts, repeated 10 times with 10 s intervals. eEPSCs and eIPSCs persisted with 20Hz stimulation, but both gradually became decreased in amplitude and conductance by about 50% over the course of the stimulus train in a roughly parallel fashion (Fig. 3a and b). In addition, the percentage of stimuli that failed to elicit responses increased during the train (Fig. 3c). There was no significant change in the EPSC:IPSC ratios, measured as either conductance or failure rate, during the course of the 20Hz frequency trains, despite the

decrease in amplitude.

3.4. Effects of hippocampal output on HPA axis function in vivo

Previous studies have shown that lesions of GABAergic cells in the BNST lead to an enhancement of HPA axis responses to acute restraint stress (Radley and Sawchenko, 2011), but it has never been shown that hippocampal activation acutely regulates the stress-response. Because our anatomical and electrophysiological data suggested that the hippocampus inhibited CRF + PVN neurons via activation of the BNST, we predicted that stimulating hippocampal afferents to the BNST and PVN would attenuate the plasma glucocorticoid response to an acute stressor. We expressed ChR-EYFP bilaterally in the ventral hippocampus of male wildtype C57/Bl6 mice, as above, and implanted two optical fibers with the fiber tips targeting the fornix region upstream of the BNST and PVN. Mice were placed in a restraint tube and connected to dual optical fibers. After 15 min, they were returned to their home cages and the fiber was detached. Blood was collected via tail snip at 0, 15, 30, 60, and 120 min after initial placement in the restraint tube. As a control for variations in ChR expression and fiber placement, a cross-over experimental design was used, in which mice received optical stimulation at 20Hz frequency 10 mW intensity in an alternating 2s on/off stimulation protocol for the duration of the 15-min acute restraint stress, or a mock-stimulation trial (Fig. 4a). The mock stimulation included all the handling and light associated with the real stimulation, but the optical pathway at the ferrule sleeve was blocked with lens tissue, reducing the measured

Fig. 3. High frequency electrical stimulation of fornix elicits currents in CRF + neurons in the PVN. **a)** Electrically evoked EPSCs (−60 mV) and IPSCs (0 mV) recorded in CRF + neuron in the PVN in response to stimulation of the fornix at 20Hz for 1 s, repeated 10 times. **b)** There was a comparable ~50% decrease in both EPSC and IPSC conductance over the duration of the stimulus train. **c)** Similarly, there was a comparable ~50% decrease in the probability that a given stimulus elicited an EPSC or IPSC over the duration of the 20Hz stimulus trains.

output intensity by more than 100-fold to <0.1 mW. The restraint and stimulation procedure were performed in two separate trials one week apart for each animal to generate within-animal paired datasets (Fig. 4a). Acute restraint stress produced a transient elevation of plasma CORT level that peaked 30–60 min after the onset of stress and declined over the following 2 h (Fig. 4b–d). Mice receiving photostimulation at 10 mW had a significant decrease in the peak stress-induced CORT levels, compared to the same animals receiving mock stimulation (Fig. 4b–d, Suppl. Fig. 2a and b). The effects of stimulation at 10 mW persisted beyond the period of stimulation, as apparent in different total areas under the curve (Fig. 4c).

To control for stimulation order, the CORT values for these mice were regrouped into whether the samples taken during the first or second trial of each mouse (Fig. 4a). No significant effect of stimulation order were observed when the data was reanalyzed in this manner (Fig. 4E-G, Suppl. Fig. 2c and d), suggesting that the strong photostimulation itself was cause for the decrease in CORT. We conclude that hippocampal output is sufficient to partially suppress acute HPA axis responses to stress.

4. Discussion

The synaptic mechanisms underlying hippocampal regulation of the HPA axis were investigated in mice. Because the hippocampus is known to be both stress-sensitive and associated with psychiatric illness, understanding its contributions to neuroendocrine regulation is important for many disease processes. The canonical hypothesis is that the hippocampus decreases stress-induced glucocorticoid production via inhibition of the CRF-releasing cells in the PVN. The major projection neurons of the hippocampus are excitatory, therefore, for this hypothesis to be true there must be one or more inhibitory brain regions interposed between the hippocampus and the PVN. The ventral hippocampus is considered to be the region of the hippocampus most responsible for processing affective information, particularly in regards to stress and anxiety and therefore was the focus of this study (Bertagna et al., 2020; Fanselow and Dong, 2010; O'Mara, 2005; Kheirbek et al., 2013).

Prior studies have suggested that the hippocampus has a high expression of glucocorticoid receptors and inhibits production of

glucocorticoids, making it a likely region for involvement in negative feedback of the HPA axis. Although the idea of the hippocampus solely mediating negative feedback of the HPA axis has fallen out of favor, the hippocampus can contribute to HPA axis regulation (Furay et al., 2008). However, the mechanisms and neural circuits underlying this response are unclear. To our knowledge there is no direct evidence of the effects of hippocampal projections on CRF-releasing cells in the PVN. It was also uncertain if hippocampal activity is even capable of inhibiting the HPA axis during acute stressors, or if it takes more a sustained and chronic perturbation in hippocampal activity to meaningfully alter the HPA axis.

Consistent with prior anatomical studies, observation of hippocampal nerve terminals labeled with virally expressed EYFP demonstrated abundant innervation of the BNST and peri-PVN region, which were previously identified as likely targets for this regulation (Radley and Sawchenko, 2011; Kishi et al., 2000). There were few hippocampal projections directly innervating the regions of the PVN where CRF + cell somata are located, also consistent with previous work (Radley and Sawchenko, 2011). It is noteworthy that a similar paucity of direct excitatory projections to the PVN, but strong projections to the BNST, has also been reported for efferents from the infralimbic (IL) or prelimbic (PL) cortex (Wood et al., 2019; Radley et al., 2009), suggesting that they produce similar effects on HPA axis function.

We used optogenetic stimulation of hippocampal efferents in transgenic reporter mice to test for synaptic responses in CRF + neurons in the PVN. Although we could clearly see both terminals and CRF + cells in the PVN within a single slice cut in the coronal plane, we were unable to optically evoke responses. Although negative results are difficult to interpret, synaptic responses were consistently evoked in parasagittal sections with the identical stimulation and recording configuration. We suggest that this may explain why these responses have not been previously described in the literature. Boudaba et al., 1996 (Boudaba et al., 1996) did evoke inhibitory responses in PVN cells in response to focal application of glutamate in the peri-PVN in coronal slices, suggesting that the GABAergic cells and their projections to the PVN remain intact in such slices. Optical stimulation of hippocampal terminals in the peri-PVN failed to produce an equivalent response, however, suggesting that hippocampus does not inhibit the PVN via activation of these peri-PVN inhibitory neurons. Other recording conditions could reveal
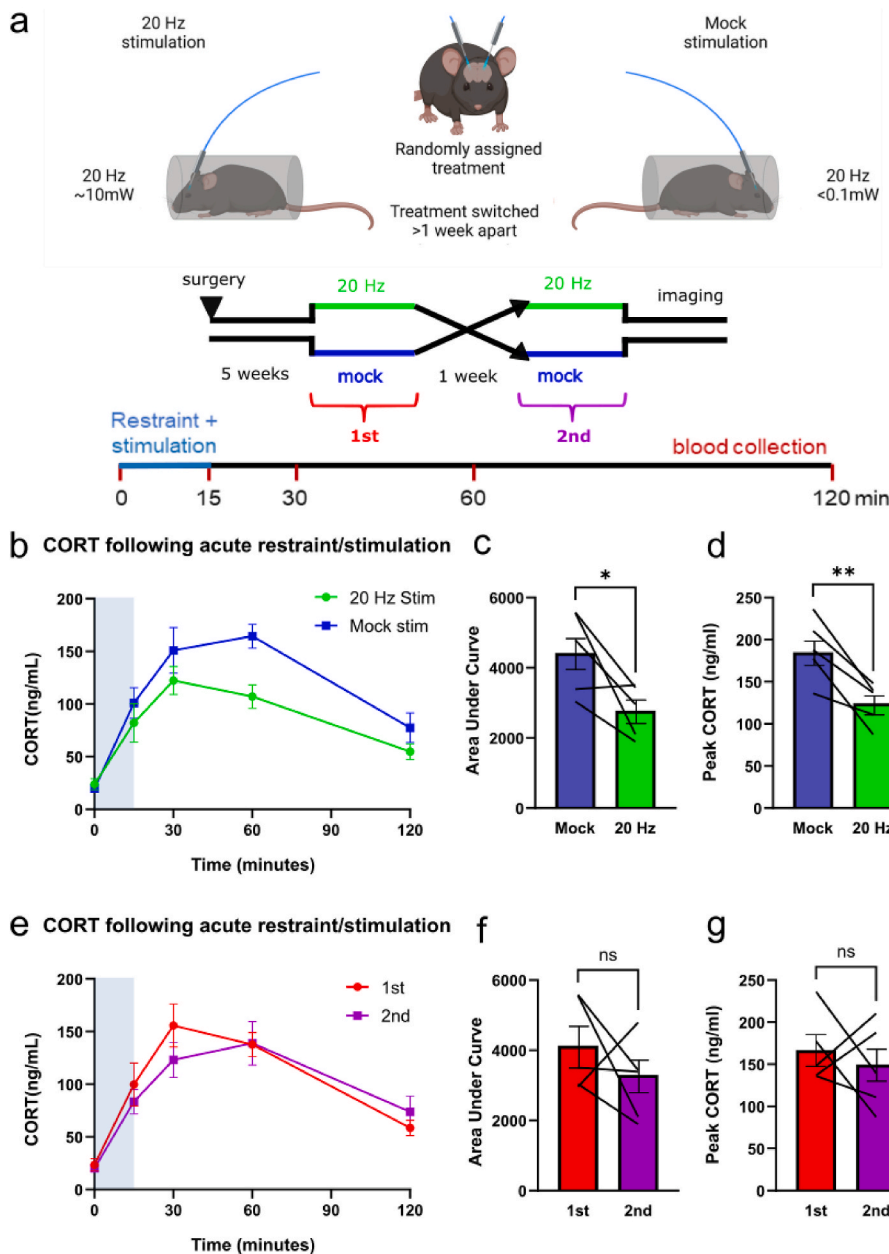
Fig. 4. Optical stimulation of hippocampal efferents suppresses the stress-induced CORT response.
a) ChR and EYFP were expressed in the CA1 region of male C57/Bl6 mice bilaterally and optical fibers targeted hippocampal terminals in the fornix anterior to the BNST. Each animal was randomly assigned to 20Hz stimulation at 10 mW or mock stimulation at 0.1 mW and the opposite treatment 1 week later. Animals were restrained for 15 min and received 20Hz optical stimulation 2 s on, 2 s off for the duration of the restraint. Blood was sampled via tail snip at 0, 15, 30, 60, and 120 min timepoints for CORT assay. **b)** Comparison of the timecourse of CORT responses in the full power and mock 20Hz stimulation trials. Mixed-effects ANOVA was performed on the resulting curve, with time effect (n = 6, $F_{2.121,20.15}$ = 31.10, p < 0.0001) and treatment effects (n = 6, $F_{1,10}$ = 5.186, p = 0.0460). **c,d)** Comparison of the area under the curve and peak CORT responses in the paired trials from b showing significant effects of hippocampal stimulation. Paired t-tests for mock vs stim AUC (n = 5, p = 0.0184) and peak value (n = 5, p = 0.0105) were significant. *, p < 0.05; **, p < 0.01. **e,f,g)** The same data after resorting by recording order demonstrating no significant effects. When segregated by order of recording, mixed effects ANOVA maintains time effect (n = 6, $F_{2.397,22.77}$ = 34.24, p < 0.0001) but loses treatment effect (n = 6, $F_{1,10}$ = 0.4163, p = 0.5333). Similarly, paired t-tests performed on recording order AUC (n = 5, p = 0.2936) and peak CORT (n = 5, p = 0.5404) were not significantly different.

occult connections that were not apparent under our conditions.

With optical stimulation in parasagittal sections, we were twice as likely to elicit inhibitory responses in CRF + cells as excitatory responses. Although there is little discussion of direct excitatory input from hippocampus to the PVN in prior literature, we did record optically evoked EPSCs in 4 of 8 recordings. In 3 of 8 cells, both excitatory and inhibitory responses were optically evoked. The latency for IPSCs was twice as long as for EPSCs, and IPSCs displayed much greater jitter, suggestive of a direct excitatory input and indirect disynaptic or polysynaptic circuit for the inhibitory inputs, though this was not tested experimentally. Despite the negligible difference in EPSC and IPSC amplitudes, IPSCs have a longer duration than EPSCS and this difference in charge transfer will contribute to powerful inhibition of CRF + cell firing.

In contrast to the responses elicited with selective optical stimulation of hippocampal afferents, electrical stimulation within the fornix elicited both EPSCs and IPSCs in 11 of 12 cells. We suggest that this difference results because electrical stimulation recruits some other,

stronger direct excitatory input to the CRF + cells in the PVN, such as from the amygdala, rather than just ventral hippocampal inputs (Prewitt and Herman, 1998). There was no evidence of a frequency-dependent shift in the ratio between excitatory and inhibitory strength with electrical stimulation, suggesting that this does not explain the net inhibitory effect of hippocampal output. Instead, the larger proportion of CRF + cells displaying inhibitory responses to stimulation of hippocampal efferents is consistent with a potent, divergent inhibitory input from the BNST and perhaps other nearby regions. This strong disynaptic input may be sufficient to explain a net inhibitory effect of hippocampal inputs to the PVN. Another possibility is that the hippocampus has multiple output streams that can alternatively activate an excitatory or inhibitory pathway to the PVN depending on the context of the stressor. There is some evidence of differential effects of subicular lesions depending on the stressor type, suggesting it may differentially play an excitatory or inhibitory role (Mueller et al., 2004).

The BNST has long been implicated as a key sign-reversing node in which excitatory output from the hippocampus is converted to

inhibition of the PVN (Herman and Mueller, 2006; Radley and Sawchenko, 2011; Herman et al., 2002, 2016; Myers et al., 2012). As predicted, we observed strong excitatory and inhibitory synaptic responses in GAD + inhibitory neurons within the BNST in response to optical stimulation of hippocampal efferents. Unlike responses in the PVN, optically evoked EPSCs and IPSCs were reliably observed in BNST neurons (7 of 7 cells) and had relatively equivalent conductances. Latency from the optical stimulus was longer for IPSCs than EPSCs, consistent with disynaptic inhibition, either feedforward or feedback. The posterior BNST is reported to inhibit PVN activity (Choi et al., 2007) and our data demonstrates that these cells, as well as some medial regions of the BNST, receive potent excitation from the ventral hippocampus. Description of BNST subregions in the sagittal plane is challenging because most descriptions are in the coronal plane. However, areas immediately posterior or inferior to the anterior commissure, in very medial parasagittal to midline sections, were the most reliable areas for recording evoked responses.

The disynaptic, sign-reversing circuit characterized above provides the potential means for the hippocampus to inhibit the HPA axis, as long postulated, although this has not been previously demonstrated. We observed that both EPSC and IPSC amplitude declined during maintained 20 Hz stimulation but were not eliminated. Furthermore, the ratio of excitatory-to-inhibitory conductance remained relatively unaffected by 20 Hz stimulation. These data suggest that sustained hippocampal output would remain largely inhibitory in PVN CRF + cells.

Using 15 min of restraint as an acute stressor, we observed that simultaneous delivery of 20 Hz optical stimulation of hippocampal afferents to the BNST region produced a significant reduction in the peak and overall elevation of circulating CORT in male mice. This effect was apparent at the cessation of the stimulation and persisted during the full 2 h of recovery. The consistent low CORT levels at timepoint 0 (<50 ng/ml) in both treatment conditions indicates that the mice remained unstressed prior to being placed in the restraint tubes. To our knowledge, this is the first demonstration that stimulation of hippocampal ioutput leads to inhibition of stress-induced HPA axis activation.

Taken together with the complimentary findings that lesions of GABAergic cells within the BNST lead to increased stress-induced HPA activation (Radley and Sawchenko, 2011) and that BNST cells inhibit PVN cells (Choi et al., 2007), we suggest that the inhibitory projection from the BNST to the PVN contributes to the inhibitory actions of hippocampal photostimulation. Other hypothalamic GABAergic cell populations may also contribute, including those in the peri-PVN region (Boudaba et al., 1996). Our findings suggest that inhibiting the BNST, for example by using halorhodopsin, should diminish or eliminate disynaptic IPSCs in PVN neurons and the effects of hippocampal stimulation on the acute stress response. Because the BNST is considered an integrator of input from many brain regions, it was not clear if hippocampus alone would be able to alter systemic levels of CORT. The effect of 20 Hz stimulation was not large, representing a <ca. 25% reduction in the full area under the curve. This suggests that there are other powerful excitatory influences on the CRF cells that the hippocampal-BNST mediated inhibition cannot fully counteract. The effect of optogenetic stimulation of IL cortical efferents produced a comparably sized effect on stress-induced CORT levels (Schaeuble et al., 2021).

These findings suggest that the role of hippocampal projections to the PVN is perhaps not to produce rapid corticosterone-dependent feedback inhibition in response to elevations in CORT levels, as has long been assumed. Indeed, canonical nuclear GRs and MRs in the hippocampus are poorly suited to mediate rapid responses and changes in hippocampal output, given the slow nature of the expected responses they produce, although putative rapid membrane signaling has been proposed (Karst et al., 2005; Di et al., 2016; Orchinik et al., 1991; Evanson et al., 2010; Hu et al., 2010; Strehl and Buttgereit, 2014). Instead, ongoing activity in hippocampal and IL cortical inputs may set an allostatic steady-state tone in the average level of excitability of PVN CRF-releasing cells. These inputs could also trigger tonic changes in PVN

tone in response to environmental conditions and features perceived through cortical processing, such as those that might demand a heightened or dampened HPA axis response. More information about the dynamics of hippocampal output to the hypothalamus in response to stress would be valuable in testing these hypotheses.

Optogenetic stimulation of IL efferents inhibits HPA axis activation only in male rats, and not in females (Wallace et al., 2021). We note that our *in vivo* experiments were only performed in male mice because we were unable to find a description of the anatomy of the BNST in female mice to guide placement of the optical fiber. Literature suggests that the female BNST is considerably smaller in volume than the male BNST in humans (Avery et al., 2014, 2016), but we found no reliable source demonstrating where these volumetric changes are concentrated in the female mouse brain. There is also a potential sex-difference in the hippocampal input to PVN as well as the multitude of other brain regions that signal to the BNST (Allen and Gorski, 1990).

The hippocampus has numerous links to both major depression and neuroendocrine regulation in clinical and preclinical literature (Thompson et al., 2015; Sapolsky, 2002; Herman et al., 2003). Using rodent models, we and others have shown there are lasting anatomical and physiological changes in hippocampal synapses following chronic stress that correlate with depression-relevant behaviors (Kallarackal et al., 2013; Magariños and McEwen, 1995). These synaptic changes are reversible following administration of antidepressant compounds and resolve with the behavioral measures (Kallarackal et al., 2013; Cai et al., 2013). Furthermore, treatment with the glucocorticoid corticosterone (CORT) was shown to mimic the behavioral and synaptic changes seen following chronic stress (Kvarta et al., 2015). Blocking endogenous production of CORT during chronic stress was able to block the stress-induced synaptic and behavioral changes. We and others have also previously shown functional significance of hippocampal projections in mediating reward-related behavior (LeGates et al., 2018; Sjulson et al., 2018; Britt et al., 2012). Our present findings suggest that dysregulation of the HPA axis, a symptom of depression, may also involve similar hippocampal mechanisms. Volumetric changes in the hippocampus are seen in patients with major depression, and lesion studies demonstrate that loss of hippocampus or the major output of hippocampus can lead to dysregulation of the neuroendocrine system (Herman et al., 1998; Sheline et al., 1996, 1999). The ventral hippocampus is of particular interest, as studies show increased connectivity to affective brain regions (for review (O'Mara, 2005),). It will be of interest to investigate the possible role of changes in hippocampal inputs to the PVN and BNST under conditions of stress-response dysregulation such, as is seen following chronic stress.

5. Conclusion

We have shown evidence that hippocampal afferents elicit monosynaptic excitation and likely disynaptic inhibition of CRF-secreting cells in the PVN and that activation of this projection can significantly inhibit the acute stress response. We also suggest that GABAergic cells in the BNST contribute to the polysynaptic inhibition of CRF + PVN cells in response to hippocampal output. Further understanding the central regulation of PVN in both normal and disease states is essential and could lead to important breakthroughs in our understanding of disease and improving treatment options.

CRediT authorship contribution statement

Anthony B. Cole: Experiments were designed, performed and analyzed, the manuscript was written. **Kristen Montgomery:** Experiments were performed and analyzed, the manuscript was written. **Tracy L. Bale:** Experiments were designed, funding was provided, the manuscript was written. **Scott M. Thompson:** Experiments were designed, the manuscript was written, funding was provided.

Declaration of competing interest

The authors whose names are listed immediately below certify that they have NO affiliations with or involvement in any organization or entity with any financial interest (such as honoraria; educational grants; participation in speakers' bureaus; membership, employment, consultancies, stock ownership, or other equity interest; and expert testimony or patent-licensing arrangements), or nonfinancial interest (such as personal or professional relationships, affiliations, knowledge or beliefs) in the subject matter or materials discussed in this manuscript.

Data availability

Data will be made available on request.

Acknowledgements

Appendix A. Supplementary data

Supplementary data to this article can be found online at https://doi.org/10.1016/j.ynstr.2022.100473.

References

Allen, L.S., Gorski, R.A., 1990. Sex difference in the bed nucleus of the stria terminalis of the human brain. J. Comp. Neurol. 302, 697–706.

Anwar, H., Li, X., Bucher, D., Nadim, F., 2017. Functional roles of short-term synaptic plasticity with an emphasis on inhibition. Curr. Opin. Neurobiol. 43, 71–78.

Avery, S.N., et al., 2014. BNST neurocircuitry in humans. Neuroimage 91, 311–323.

Avery, S.N., Clauss, J.A., Blackford, J.U., 2016. The human BNST: functional role in anxiety and addiction. Neuropsychopharmacology 41, 126–141.

Bale, T.L., Vale, W.W., 2004. CRF and CRF receptors: role in stress responsivity and other behaviors. Annu. Rev. Pharmacol. Toxicol. 44, 525–557.

Bertagna, N.B., et al., 2020. Involvement of the ventral, but not dorsal, hippocampus in anxiety-like behaviors in mice exposed to the elevated plus maze: participation of CRF1 receptor and PKA pathway. Pharmacol. Rep. 73, 57–72.

Boudaba, C., Szabó, K., Tasker, J.G., 1996. Physiological mapping of local inhibitory inputs to the hypothalamic paraventricular nucleus. J. Neurosci. 16, 7151–7160.

Boyden, E.S., Zhang, F., Bamberg, E., Nagel, G., Deisseroth, K., 2005. Millisecond-timescale, genetically targeted optical control of neural activity. Nat. Neurosci. 8, 1263–1268.

Britt, J.P., et al., 2012. Synaptic and behavioral profile of multiple glutamatergic inputs to the nucleus accumbens. Neuron 76, 790–803.

Cai, X., et al., 2013. Local potentiation of excitatory synapses by serotonin and its alteration in rodent models of depression. Nat. Neurosci. 16, 464–472.

Choi, D.C., et al., 2007. Bed nucleus of the stria terminalis subregions differentially regulate hypothalamic-pituitary-adrenal axis activity: implications for the integration of limbic inputs. J. Neurosci. 27, 2025–2034.

Cullinan, W.E., Herman, J.P., Watson, S.J., 1993. Ventral subicular interaction with the hypothalamic paraventricular nucleus: evidence for a relay in the bed nucleus of the stria terminalis. J. Comp. Neurol. 332, 1–20.

Cullinan, W.E., Ziegler, D.R., Herman, J.P., 2008. Functional role of local GABAergic influences on the HPA axis. Brain Struct. Funct. 213, 63–72.

Daigle, T.L., et al., 2018. A suite of transgenic driver and reporter mouse lines with enhanced brain-cell-type targeting and functionality. Cell 174, 465–480 e22.

Di, S., et al., 2016. Acute stress suppresses synaptic inhibition and increases anxiety via endocannabinoid release in the basolateral amygdala. J. Neurosci. 36, 8461–8470.

Dong, H.W., Swanson, L.W., 2003. Projections from the rhomboid nucleus of the bed nuclei of the stria terminalis: implications for cerebral hemisphere regulation of ingestive behaviors. J. Comp. Neurol. 463, 434–472.

Dong, H.W., Swanson, L.W., 2004a. Organization of axonal projections from the anterolateral area of the bed nuclei of the stria terminalis. J. Comp. Neurol. 468, 277–298.

Dong, H.W., Swanson, L.W., 2004b. Projections from bed nuclei of the stria terminalis, posterior division: implications for cerebral hemisphere regulation of defensive and reproductive behaviors. J. Comp. Neurol. 471, 396–433.

Dong, H.W., Swanson, L.W., 2006a. Projections from bed nuclei of the stria terminalis, anteromedial area: cerebral hemisphere integration of neuroendocrine, autonomic, and behavioral aspects of energy balance. J. Comp. Neurol. 494, 142–178.

Dong, H.W., Swanson, L.W., 2006b. Projections from bed nuclei of the stria terminalis, magnocellular nucleus: implications for cerebral hemisphere regulation of micturition, defecation, and penile erection. J. Comp. Neurol. 494, 108–141.

Dong, H.W., Swanson, L.W., 2006c. Projections from bed nuclei of the stria terminalis, dorsomedial nucleus: implications for cerebral hemisphere integration of neuroendocrine, autonomic, and drinking responses. J. Comp. Neurol. 494, 75–107.

Dong, H.W., Petrovich, G.D., Swanson, L.W., 2000. Organization of projections from the juxtacapsular nucleus of the BST: a PHAL study in the rat. Brain Res. 859, 1–14.

Dong, H.W., Petrovich, G.D., Swanson, L.W., 2001. Topography of projections from amygdala to bed nuclei of the stria terminalis. Brain Res. Rev. 38, 192–246.

Evanson, N.K., Tasker, J.G., Hill, M.N., Hillard, C.J., Herman, J.P., 2010. Fast feedback inhibition of the HPA axis by glucocorticoids is mediated by endocannabinoid signaling. Endocrinology 151, 4811–4819.

Fanselow, M.S., Dong, H.W., 2010. Are the dorsal and ventral Hippocampus functionally distinct structures? Neuron 65, 7–19.

Furay, A.R., Bruestle, A.E., Herman, J.P., 2008. The role of the forebrain glucocorticoid receptor in acute and chronic stress. Endocrinology 149, 5482–5490.

Gergues, M.M., et al., 2020. Circuit and molecular architecture of a ventral hippocampal network. Nat. Neurosci. 23, 1444–1452.

Harris, J.A., et al., 2019. Hierarchical organization of cortical and thalamic connectivity. Nature 575, 195–202.

Herman, J.P., Cullinan, W.E., 1997. Neurocircuitry of stress: central control of the hypothalamic-pituitary-adrenocortical axis. Trends Neurosci. 20, 78–84.

Herman, J.P., Mueller, N.K., 2006. Role of the ventral subiculum in stress integration. Behav. Brain Res. 174, 215–224.

Herman, J.P., Cullinan, W.E., Young, E.A., Akil, H., Watson, S.J., 1992. Selective forebrain fiber tract lesions implicate ventral hippocampal structures in tonic regulation of paraventricular nucleus corticotropin-releasing hormone (CRH) and arginine vasopressin (AVP) mRNA expression. Brain Res. 592, 228–238.

Herman, J.P., Dolgas, C.M., Carlson, S.L., 1998. Ventral subiculum regulates hypothalamo-pituitary-adrenocortical and behavioural responses to cognitive stressors. Neuroscience 86, 449–459.

Herman, J.P., Tasker, J.G., Ziegler, D.R., Cullinan, W.E., 2002. Local circuit regulation of paraventricular nucleus stress integration: glutamate-GABA connections. Pharmacol. Biochem. Behav. 71, 457–468.

Herman, J.P., et al., 2003. Central mechanisms of stress integration: hierarchical circuitry controlling hypothalamo-pituitary-adrenocortical responsiveness. Front. Neuroendocrinol. 24, 151–180.

Herman, J.P., et al., 2016. Regulation of the hypothalamic-pituitary- adrenocortical stress response. Compr. Physiol. 6, 603–621.

Holsboer, F., 2000. The corticosteroid receptor hypothesis of depression clinical evidence. Neuropsychopharmacology 23, 477–501.

Hu, W., Zhang, M., Czéh, B., Flügge, G., Zhang, W., 2010. Stress impairs GABAergic network function in the hippocampus by activating nongenomic glucocorticoid receptors and affecting the integrity of the parvalbumin-expressing neuronal network. Neuropsychopharmacology 35, 1693–1707.

Ikeda, Y., Kumagai, H., Skach, A., Sato, M., Yanagisawa, M., 2013. Modulation of circadian glucocorticoid oscillation via adrenal Opioid-CXCR7 Signaling alters emotional behavior. Cell 155, 1323–1336.

Johnson, S.B., et al., 2016. A basal forebrain site coordinates the modulation of endocrine and behavioral stress responses via divergent neural pathways. J. Neurosci. 36, 8687–8699.

Johnson, S.B., et al., 2019. Prefrontal–bed nucleus circuit modulation of a passive coping response set. J. Neurosci. 39, 1405–1419.

Kallarackal, A.J., et al., 2013. Chronic stress induces a selective decrease in AMPA receptor-mediated synaptic excitation at hippocampal temporoammonic-CA1 synapses. J. Neurosci. 33, 15669–15674.

Karst, H., et al., 2005. Mineralocorticoid receptors are indispensable for nongenomic modulation of hippocampal glutamate transmission by corticosterone. Proc. Natl. Acad. Sci. U. S. A 102, 19204–19207.

Kathol, G., Jaeckle, S., Meller, H., Lopez, F., 1989. Pathophysiology of HPA Axis Abnormalities in patients with major depression: an update. Am. J. Psychiatr. 311–317.

Kheirbek, M.A., et al., 2013. Differential control of learning and anxiety along the dorsoventral axis of the dentate gyrus. Neuron 77, 955–968.

Kim, S.Y., et al., 2013. Diverging neural pathways assemble a behavioural state from separable features in anxiety. Nature 496, 219–223.

Kishi, T., et al., 2000. Topographical organization of projections from the subiculum to the hypothalamus in the rat. J. Comp. Neurol. 419, 205–222.

Kvarta, M.D., Bradbrook, K.E., Dantrassy, H.M., Bailey, A.M., Thompson, S.M., 2015. Corticosterone mediates the synaptic and behavioral effects of chronic stress at rat hippocampal temporoammonic synapses. J. Neurophysiol. 114, 1713–1724.

Larsen, R.S., Sjöström, P.J., 2015. Synapse-type-specific plasticity in local circuits. Curr. Opin. Neurobiol. 35, 127–135.

Lebow, M.A., Chen, A., 2016. Overshadowed by the amygdala: the bed nucleus of the stria terminalis emerges as key to psychiatric disorders. Mol. Psychiatr. 21, 450–463.

LeGates, T.A., et al., 2018. Reward behaviour is regulated by the strength of hippocampus–nucleus accumbens synapses. Nature 564, 258–262.

Lein, E.S., et al., 2007. Genome-wide atlas of gene expression in the adult mouse brain. Nature 445, 168–176.

Lightman, S.L., Conway-Campbell, B.L., 2010. The crucial role of pulsatile activity of the HPA axis for continuous dynamic equilibration. Nat. Rev. Neurosci. 11, 710–718.

Lingg, R.T., et al., 2020. Bed nuclei of the stria terminalis modulate memory consolidation via glucocorticoid-dependent and -independent circuits. Proc. Natl. Acad. Sci. USA 117, 201915501.

Lowry, C.A., 2002. Functional subsets of serotonergic neurones: implications for control of the hypothalamic-pituitary-adrenal axis. J. Neuroendocrinol. 14, 911–923.

Madisen, L., et al., 2010. A robust and high-throughput Cre Repooting and characterization. Nat. Neurosci. 13, 133–140.

Magariños, A.M., McEwen, B.S., 1995. Stress-induced atrophy of apical dendrites of hippocampal CA3c neurons: comparison of stressors. Neuroscience 69, 83–88.

Magarinos, A.M., Somoza, G., De Nicola, A.F., 1987. Glucocorticoid negative feedback and glucocorticoid receptors after hippocampectomy in rats. Horm. Metab. Res. 19, 105–109.

Maggio, N., Segal, M., 2009. Differential corticosteroid modulation of inhibitory synaptic currents in the dorsal and ventral hippocampus. J. Neurosci. 29, 2857–2866.

Morrison, K.E., et al., 2020. Pubertal adversity alters chromatin dynamics and stress circuitry in the pregnant brain. Neuropsychopharmacology 45, 1263–1271.

Motulsky, H.J., Brown, R.E., 2006. Detecting outliers when fitting data with nonlinear regression - a new method based on robust nonlinear regression and the false discovery rate. BMC Bioinf. 7, 1–20.

Mueller, N.K., Dolgas, C.M., Herman, J.P., 2004. Stressor-selective role of the ventral subiculum in regulation of neuroendocrine stress responses. Endocrinology 145, 3763–3768.

Myers, B., McKlveen, J.M., Herman, J.P., 2012. Neural regulation of the stress response: the many faces of feedback. Cell. Mol. Neurobiol. 32, 683–694.

Oh, S.W., et al., 2014. A mesoscale connectome of the mouse brain. Nature 508, 207–214.

Orchinik, M., Murray, T.F., Moore, F.L., 1991. A corticosteroid receptor in neuronal membranes. Science 252, 1848–1851.

O'Mara, S., 2005. The subiculum: what it does, what it might do, and what neuroanatomy has yet to tell us. J. Anat. 207, 271–282.

Pariante, C.M., Lightman, S.L., 2008. The HPA axis in major depression: classical theories and new developments. Trends Neurosci. 31, 464–468.

Paxinos, G., Franklin, K.B.J., 2007. The Mouse Brain in Stereotaxis Coordinates. Academic Press.

Prewitt, C.M.f., Herman, J.P., 1998. Anatomical interactions between the central amygdaloid nucleus and the hypothalamic paraventricular nucleus of the rat: a dual tract-tracing analysis. J. Chem. Neuroanat. 15, 173–186.

Radley, J.J., Sawchenko, P.E., 2011. A common substrate for prefrontal and hippocampal inhibition of the neuroendocrine stress response. J. Neurosci. 31, 9683–9695.

Radley, J.J., Gosselink, K.L., Sawchenko, P.E., 2009. A discrete GABAergic relay mediates medial prefrontal cortical inhibition of the neuroendocrine stress response. J. Neurosci. 29, 7330–7340.

Ronchetti, S., Migliorati, G., Bruscoli, S., Riccardi, C., 2018. Defining the role of glucocorticoids in inflammation. Clin. Sci. 132, 1529–1543.

Russell, G., Lightman, S., 2019. The human stress response. Nat. Rev. Endocrinol. 15, 525–534.

Sapolsky, R.M., 2002. Chicken, eggs and hippocampal atrophy. Nat. Neurosci. 5, 1111–1113.

Schaeuble, D., et al., 2021. Sexually divergent cortical control of affective-autonomic integration. Faseb. J. 35.

Schouten, M., et al., 2020. Circadian glucocorticoid oscillations preserve a population of adult hippocampal neural stem cells in the aging brain. Mol. Psychiatr. 25, 1382–1405.

Sharma, S.T., Nieman, L.K., 2011. Cushing's syndrome: all variants, detection, and treatment. Endocrinol Metab. Clin. N. Am. 40, 379–391.

Sheline, Y.I., Wang, P.W., Gado, M.H., Csernansky, J.G., Vannier, M.W., 1996. Hippocampal atrophy in recurrent major depression. Proc. Natl. Acad. Sci. U. S. A 93, 3908–3913.

Sheline, Y.I., Sanghavi, M., Mintun, M.A., Gada, M.H., 1999. Depression duration but not age predicts hippocampal volume loss in medically healthy women with recurrent major depression. J. Neurosci. 19, 5034–5043.

Sjulson, L., Peyrache, A., Cumpelik, A., Cassataro, D., Buzsáki, G., 2018. Cocaine place conditioning strengthens location-specific hippocampal coupling to the nucleus accumbens. Neuron 98, 926–934 e5.

Sonino, N., Fava, G.A., 2001. Psychiatric disorders associated with cushing's syndrome. CNS Drugs 15, 361–373.

Sparta, D.R., et al., 2012. Construction of implantable optical fibers for long-term optogenetic manipulation of neural circuits. Nat. Protoc. 7, 12–23.

Spencer, R.L., Deak, T., 2017. A users guide to HPA axis research. Physiol. Behav. 178, 43–65.

Spiga, F., Walker, J.J., Terry, J.R., Lightman, S.L., 2014. HPA axis-rhythms. Compr. Physiol. 4, 1273–1298.

Strehl, C., Buttgereit, F., 2014. Unraveling the functions of the membrane-bound glucocorticoid receptors: first clues on origin and functional activity. Ann. N. Y. Acad. Sci. 1–6. https://doi.org/10.1111/nyas.12364.

Taniguchi, H., et al., 2011. A resource of cre driver lines for genetic targeting of GABAergic neurons in cerebral cortex. Neuron 71, 995–1013.

Thompson, S.M., et al., 2015. An excitatory synapse hypothesis of depression. Trends Neurosci. 38, 279–294.

Ting, J.T., Daigle, T.L., Chen, Q., Feng, G., 2014. Acute brain slice methods for adult and aging animals: application of targeted patch clamp analysis and optogenetics. Methods Mol. Biol. 1183, 221–242.

Ung, K., Arenkiel, B.R., 2012. Fiber-optic implantation for chronic optogenetic stimulation of brain tissue. JoVE 1–6. https://doi.org/10.3791/50004.

Vale, W., Spiess, J., Rivier, C., Rivier, J., 1981. Characterization of a 41-residue ovine hypothalamic peptide that stimulates secretion of corticotropin and β-endorphin. Science 213, 1394–1397.

Wallace, T., et al., 2021. Sexually divergent cortical control of affective-autonomic integration. Psychoneuroendocrinology 129, 105238.

Wamsteeker Cusulin, J.I., Füzesi, T., Watts, A.G., Bains, J.S., 2013. Characterization of corticotropin-releasing hormone neurons in the paraventricular nucleus of the hypothalamus of crh-IRES-cre mutant mice. PLoS One 8, e64943.

Wang, X., Zhang, C., Szábo, G., Sun, Q.Q., 2013. Distribution of CaMKIIα expression in the brain in vivo, studied by CaMKIIα-GFP mice. Brain Res. 1518, 9–25.

Wood, M., et al., 2019. Infralimbic prefrontal cortex structural and functional connectivity with the limbic forebrain: a combined viral genetic and optogenetic analysis. Brain Struct. Funct. 224, 73–97.